

Molecular dynamics investigation of viscosity, chemical diffusivities and partial molar volumes of liquids along the MgO–SiO₂ join as functions of pressure

Daniel J. Lacks^a, David B. Rear^a, James A. Van Orman^{b,*}

^a Department of Chemical Engineering, Case Western Reserve University, Cleveland, OH 44106, USA

^b Department of Geological Sciences, Case Western Reserve University, Cleveland, OH 44106, USA

Received 20 July 2006; accepted in revised form 29 November 2006

Abstract

Molecular dynamics simulations are carried out to systematically address the effects of composition and pressure on melts along the MgO–SiO₂ join and elucidate the role of structural modifier content on silicate melt properties. The MgO–SiO₂ system shows non-ideal mixing with a negative excess volume of mixing at low pressures, but the mixing becomes closer to ideal at higher pressures. At atmospheric pressure, the viscosities and diffusivities vary by more than 3 orders of magnitude as the composition is varied along this join, with the low SiO₂ melts characterized by lower viscosities and higher diffusivities; these results are in quantitative agreement with experimental results for the dependence of viscosity and diffusivity on structural modifier content in a wide range of silicate systems. The transport properties of melts in this system converge at higher pressures; at pressures greater than ~15 GPa the viscosity and diffusivities vary by less than an order of magnitude across the entire range of compositions. The relevance of equations that relate the viscosity and diffusivity is also addressed.

© 2006 Elsevier Inc. All rights reserved.

1. Introduction

Knowledge of the physical and chemical properties of silicate melts is essential for understanding the formation and motion of magmas. Silicate melts span a wide range of composition, and igneous processes span a wide range of pressures and temperatures, possibly extending to conditions at Earth's core-mantle boundary (e.g., Lay et al., 2004). The properties of silicate melts at very high pressures and temperatures are particularly important for understanding the behavior of deep magma oceans, which are likely to have played a key role in the early thermal and chemical evolution of the Earth (Abe, 1997; Karato and Murthy, 1997; Rubie et al., 2003).

Silicate melt properties are poorly known at very high pressures due to the difficulty in performing experiments

at these conditions. High-pressure data are particularly sparse for transport properties such as viscosity and chemical diffusivity, although data have been obtained recently at pressures up to 15 GPa (Poe et al., 1997; Reid et al., 2001, 2003; Liebske et al., 2005). Extrapolating transport property data to higher pressures is perilous because silicate liquids tend to exhibit complicated behavior under compression. The viscosities of many silicate melts anomalously decrease with pressure over a certain pressure range (Scarfe et al., 1987; Suzuki et al., 2002; Behrens and Schulte, 2003; Reid et al., 2003; Tinker et al., 2004; Liebske et al., 2005). Similarly, chemical diffusion coefficients often increase with pressure (Mikkelsen, 1984; Shimizu and Kushiro, 1984; Leshner et al., 1996; Poe et al., 1997; Reid et al., 2001; Tinker and Leshner, 2001; Tinker et al., 2003). This behavior contrasts with that of minerals, in which atomic transport rates usually decrease monotonically with pressure (e.g., Van Orman et al., 2003). Although it is clear that the anomalous behavior of silicate liquids is related to

* Corresponding author.

E-mail address: james.vanorman@case.edu (J.A. Van Orman).

structural changes in the polymerized network under compression (e.g., Shimizu and Kushiro, 1984; Scarfe et al., 1987), a detailed understanding of the controls on melt transport properties remains elusive.

The most important feature of silicate melt structure is believed to be the degree of polymerization, where “polymerized” denotes that continuous chains of connected SiO₄ tetrahedra percolate throughout the system (e.g., Mysen, 1988). The degree of polymerization exerts an important control on physical properties, with less polymerized liquids generally having enhanced transport properties. Various parameters have been put forward to describe silicate melt structure. In this paper, following Giordano and Dingwell (2003), we use a very simple parameter, SM, which denotes the mole percentage of “structure modifying” oxides (i.e., all oxides other than SiO₂ and Al₂O₃).

The densities of silicate liquids have been measured over a greater range of pressure and composition than the transport properties. However, to model accurately the density of silicate liquids over the large compositional range of geological interest requires information on the partial molar volumes of melt components, and these are much less well known, especially at high pressures. Even at atmospheric pressure, non-ideal mixing between MgO and SiO₂ is not well constrained (Courtial and Dingwell, 1999) due to the difficulty in performing experiments on refractory MgO-rich liquids at the necessary high temperatures.

In this paper, molecular dynamics simulations are used to investigate systematically the dependence of melt properties on composition and pressure in liquids along the MgO–SiO₂ join (i.e., $x\text{MgO}-(1-x)\text{SiO}_2$). SiO₂ and MgO are the two most abundant oxides in Earth’s mantle, together comprising more than 80% of Earth’s mantle by mass (McDonough and Sun, 1995), and liquids in this system span a wide range of network structures, from fully polymerized to fully depolymerized. In these simulations, parameterized force fields rather than *ab initio* electronic structure calculations are used to describe the interatomic forces. This approach is less rigorous than the *ab initio* approach (e.g., Stixrude and Karki, 2005), but allows much larger systems to be simulated for much longer times, which in practice enables us to calculate melt transport properties at temperatures more relevant to Earth’s mantle. Six different compositions are considered, with $x = 0, 0.1, 1/3, 1/2, 2/3$, and 1, at 3000 K and pressures up to 50 GPa.

2. Computational methods

The basic molecular dynamics (MD) method numerically integrates Newton’s equations of motion to obtain the trajectory of the atoms. In practice, modified equations of motion are often used in order to simulate a system at constant temperature rather than constant energy. The equations of motion require as input the forces that the

atoms exert on each other; the force field used to calculate these forces in the present simulations is described below.

The MD simulations are carried out using a code written and subsequently modified by the first author (e.g., Lacks, 1998). Simulations are performed at constant volume V and temperature T , with the temperature controlled by a Nose-Hoover thermostat (Allen and Tildesley, 1989). The Runge-Kutta method, with a time step of 2 fs, is used for the numerical integration of the equations of motion, and the total time considered in each simulation is 1 ns. The simulations are carried out in an orthogonal simulation cell with periodic boundary conditions, and coulombic interactions are summed by the Ewald method. The simulations are carried out with 2160 atoms for the $x\text{MgO}-(1-x)\text{SiO}_2$ systems with $x = 0, 0.1, 1/3$ and $1/2$; 2163 atoms for the system with $x = 2/3$; and 1728 atoms for the system with $x = 1$ (pure MgO).

2.1. Force field

The simulations use the BKS force field (van Beest et al., 1990), with modifications as described below. This force field is used because it adequately models the structure and properties of a variety of silica phases, and the absence of harmonic bond stretching and angle bending terms allows the bond breaking processes associated with diffusion. The potential energy, U , is pairwise additive,

$$U = \sum_{i=1}^N \sum_{j=i+1}^N U_{ij}(r_{ij}) \quad (1)$$

where the energy for the interaction of atoms i and j separated by the distance r , $U_{ij}(r)$, is given by,

$$U_{ij}(r) = A_{ij}e^{-b_{ij}r} - \frac{C_{ij}}{r^6} + \frac{q_i q_j}{r} \quad (2)$$

The parameters A_{ij} and C_{ij} are zero for cation–cation interactions. The atomic charges q_i for Si and O, and the parameters A , b , C for Si–O and O–O interactions, are given in van Beest et al. (1990).

The modifications to the original BKS model are as follows:

- (i) a steep repulsive wall, U' , that is significant only at very short interatomic distances is added to the interatomic potential, following Saika-Voivod et al. (2001). This repulsive wall is of the form,

$$U'_{ij}(r) = \varepsilon_{ij} \left[\left(\frac{\sigma_{ij}}{r} \right)^{30} - \left(\frac{\sigma_{ij}}{r} \right)^6 \right] \quad (3)$$

where ε scales the energy and σ scales the distance, and is added to the interatomic potential given in Eq. (2). The values of ε_{ij} and σ_{ij} for Si–O and O–O interactions, are given in Saika-Voivod et al. (2001). This term is necessary because the repulsive wall of the BKS potential (Eq. (2)) has only a finite height at a finite interatomic separation, after which it

unphysically diverges to negative infinity at very short interatomic distances; in high temperature MD simulations, atoms would occasionally surmount this barrier and cause the simulations to crash. This steep wall is negligible at the interatomic distances of most interest, and so it does not alter significantly the values of properties obtained from the simulations.

- (ii) The non-coulombic potential is truncated at 5.5 Å, and shifted in energy such that the energy is continuous at this cutoff distance. This truncation, which follows Horbach and Kob (1999), leads to densities in better agreement with experiment and also reduces the computational burden of the simulations.
- (iii) Potential parameters are obtained for Mg–O interactions by fitting to experimental pressure–volume data for crystalline MgO to 52 GPa (Speziale et al., 2001). To maintain charge neutrality, the charge of the Mg ion is taken as the negative of the charge on the O ion. The values obtained for the Mg–O interactions are $A = 315,001$ kJ/mol, $b = 3.79749$ angst⁻¹, and $C = -9648.5$ kJ/molangst⁶. Note that cation–cation non-Coulombic interactions are assigned to be zero in the BKS model. The short-range repulsive wall was added for the Mg–O interaction by using the same value of ϵ as for the Si–O interaction, with the value of σ chosen to maintain a monotonically increasing repulsive wall.

2.2. Calculation of properties

The pressure and viscosity are determined from results for the stress tensor, $\sigma_{\alpha\beta}$:

$$\sigma_{\alpha\beta} = \frac{1}{V} \left\{ \sum_{i=1}^N m_i v_{\alpha,i} v_{\beta,i} - \sum_{i=1}^N \sum_{j=1+1}^N \left(\frac{x_{\alpha,i} - x_{\alpha,j}}{r_{ij}} \right) \times \left(\frac{x_{\beta,i} - x_{\beta,j}}{r_{ij}} \right) \frac{\partial U}{\partial r_{ij}} \right\} \quad (4)$$

where $v_{\alpha,i}$ is the velocity of atom i along the α axis, $x_{\alpha,i}$ is the coordinate of atom i along the α axis, r_{ij} is the distance between atoms i and j , and U is the potential energy.

The pressure is obtained as the average of the diagonal components of the stress tensor,

$$P = \frac{1}{3} (\langle \sigma_{11} \rangle + \langle \sigma_{22} \rangle + \langle \sigma_{33} \rangle) \quad (5)$$

where the brackets $\langle \dots \rangle$ designate an ensemble average. The statistical error in the pressure is estimated from the variation in the results for σ_{xx} , σ_{yy} , and σ_{zz} .

The viscosity, η , is calculated from the Green-Kubo relation (Allen and Tildesley, 1989), which involves the integral over time of the stress autocorrelation function for the off-diagonal components of the stress tensor,

$$\eta_{xy} = \frac{V}{kT} \int_0^\infty dt \langle \sigma_{xy}(t) \sigma_{xy}(0) \rangle \quad (6)$$

This ensemble averaging is carried out by evaluating this integrand with different time origins, and the upper-limit of the integral is taken to be a time large enough that

$\langle \sigma_{xy}(t) \sigma_{xy}(0) \rangle = 0$. The statistical error in the viscosity is estimated from the variation in the results for η_{xy} , η_{yz} , and η_{zx} .

The diffusion constant, D , for each element is obtained from the Einstein relation,

$$D_{\alpha,i} = \frac{\langle [x_\alpha(t) - x_\alpha(0)]^2 \rangle_i}{2t} \quad t \rightarrow \infty \quad (7)$$

where subscript α denotes diffusion in the x , y or z direction, and the brackets $\langle \dots \rangle_i$ designate an average over all atoms of type i . This relation is valid when t is large, such that non-diffusive motion at shorter times makes a negligible contribution to the overall motion of atoms. In practice, the diffusion constants are determined from the slope of $[x_\alpha(t) - x_\alpha(0)]^2$ with respect to t , for ranges of t within the diffusive regime. The error is estimated from the variation in the results for D_x , D_y , and D_z (since liquids are isotropic with respect to diffusion).

3. Results

The raw data from the simulations are shown for several cases in Figs. 1–3, in order to demonstrate the level of convergence of the properties. Four sets of raw data are shown, for the system with the fastest dynamics (MgO at 2.2 g/cm³), and the three systems with the slowest dynamics (SiO₂ at 2.36 g/cm³, SiO₂ at 2.50 g/cm³, and the $x = 0.1$ system at 2.2 g/cm³). The SiO₂ and $x = 0.1$ systems represent the worst cases in terms of the convergence of properties. MgO results are given for comparison to show the behavior of a well-converged system.

Diagonal components of the stress tensor, shown in Fig. 1, are used to determine pressures (via Eq. (5)). When converged, the stress tensor components oscillate about time-independent values. For SiO₂ at 2.36 g/cm³, it is not clear whether the stress tensor results are fully converged; for the other simulations, the results for the stress tensor do appear to have converged.

Autocorrelation functions of off-diagonal components of the stress tensor, shown in Fig. 2, are used to determine viscosities (via Eq. (6)). For SiO₂ at 2.36 g/cm³, the autocorrelation function does not decay to zero until over 400 ps; therefore, the viscosity can be obtained for this system in a 1 ns simulation, but the accuracy is limited. The autocorrelation functions for the two simulations with the next slowest dynamics decay to zero within 100 ps, so the viscosity results for these simulations should be reasonably accurate.

Mean-squared displacements, shown in Fig. 3, are used to determine diffusivities (via Eq. (7)). The use of Eq. (2) is appropriate when the dynamics are in the diffusive regime, which is characterized, on a log–log plot of mean-squared displacement vs. time, by a line with slope equal to one. Fig. 3 shows that the simulations reach the diffusive regime within the timescales of the simulation, with the exception of SiO₂ at 2.36 g/cm³. Since the simulation of SiO₂ at

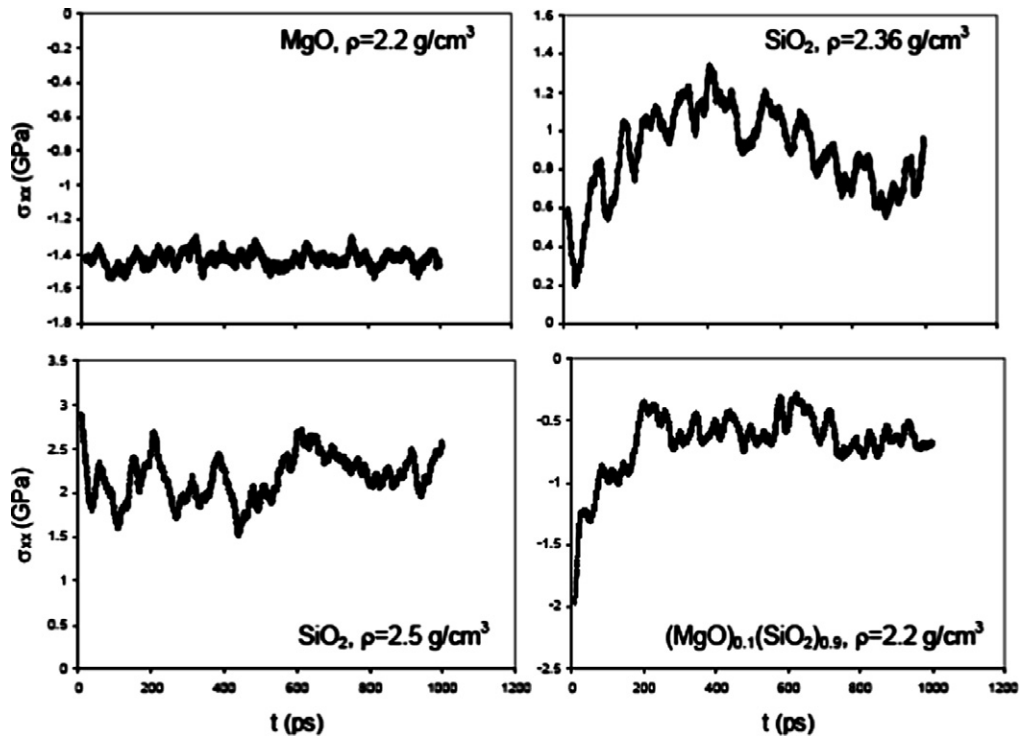


Fig. 1. Diagonal component of the stress tensor as a function of time, for four simulations.

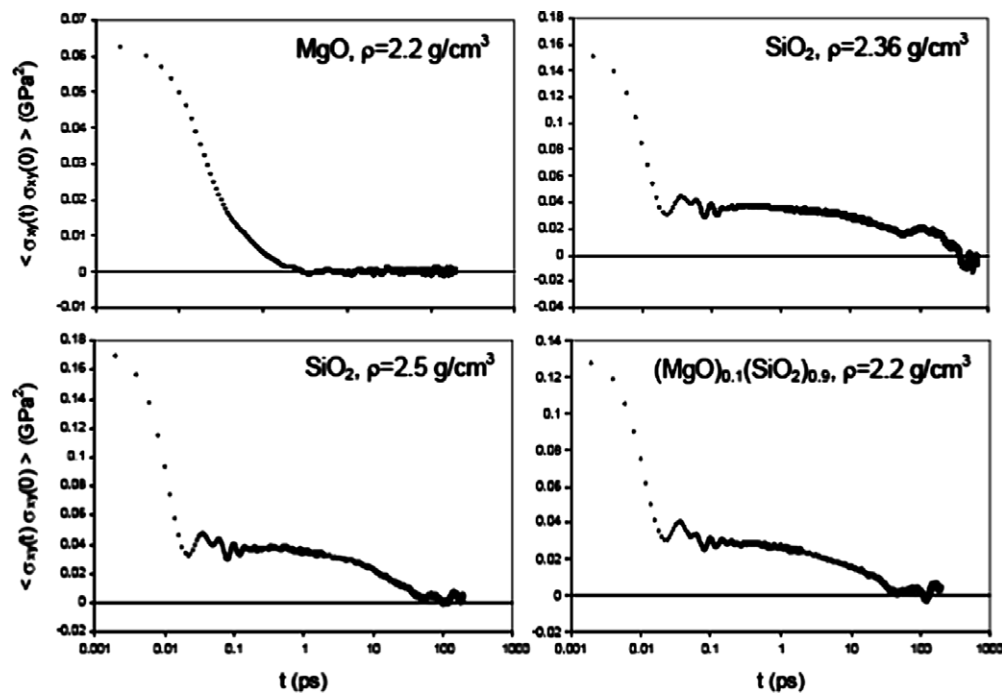


Fig. 2. Autocorrelation function for an off-diagonal component of the stress tensor, for four simulations.

2.36 g/cm³ does not fully reach the diffusive regime, the value obtained for the diffusivity in this simulation is an upper bound for the actual value.

This analysis of the raw simulation data demonstrates that, with the exception of SiO₂ at 2.36 g/cm³, the simulation results are fully converged. Note that the simulations

not shown all have dynamics that are faster than SiO₂ at 2.50 g/cm³ and the $x = 0.1$ system at 2.2 g/cm³, and so these simulations will be fully converged as well. The results for SiO₂ at 2.36 g/cm³ are at the limits of what may be considered converged, and therefore may not be as reliable as the other results.

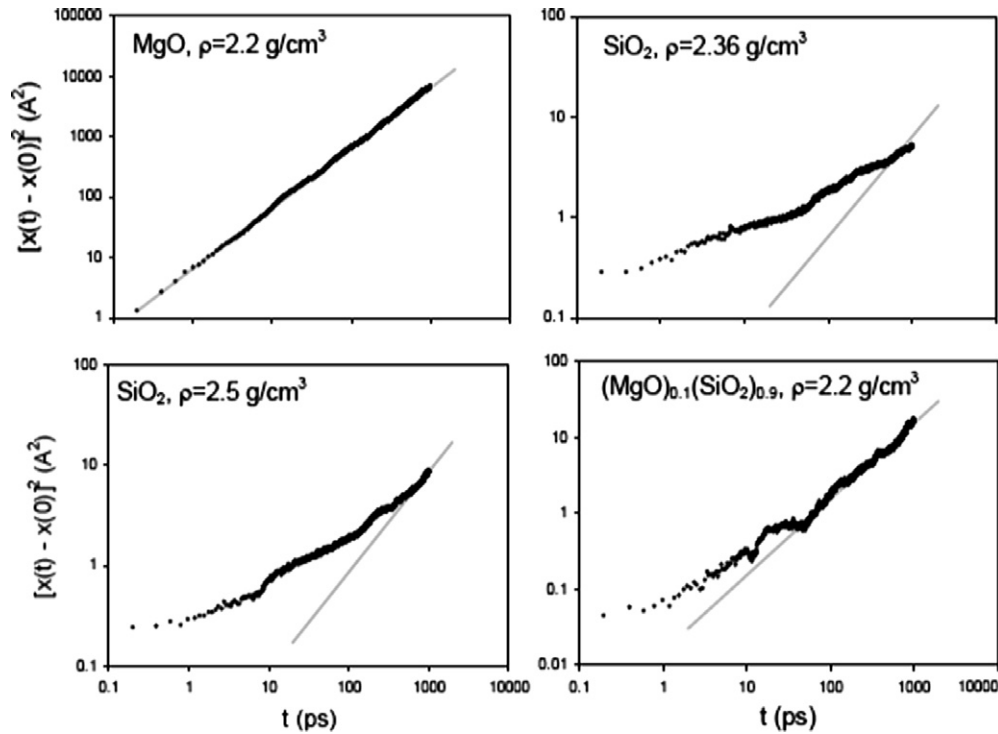


Fig. 3. Mean-squared displacement of O along one dimension as a function of time, for four simulations. The solid gray line shows the slope of one, which is characteristic of the diffusive regime.

The results for the pressure as a function of density are shown in Fig. 4. For SiO_2 , results are not obtained for densities less than 2.36 g/cm^3 , because the slow dynamics preclude equilibration on the timescales of the simulation at these densities. For MgO , results are not obtained for densities greater than 3.4 g/cm^3 , because partial crystallization occurs during simulations at high densities (the crystallization is evident in the radial distribution function).

The properties of the silicate melts are addressed below first at zero pressure, which differs negligibly from

atmospheric pressure for these systems. The pressure dependence of the properties is then addressed. Property data extracted from the simulation results for each melt composition are listed in Table 1.

3.1. Zero-pressure properties

Interpolation is necessary to obtain values for the zero pressure properties, because the simulations are carried out at constant volume rather than constant pressure – linear

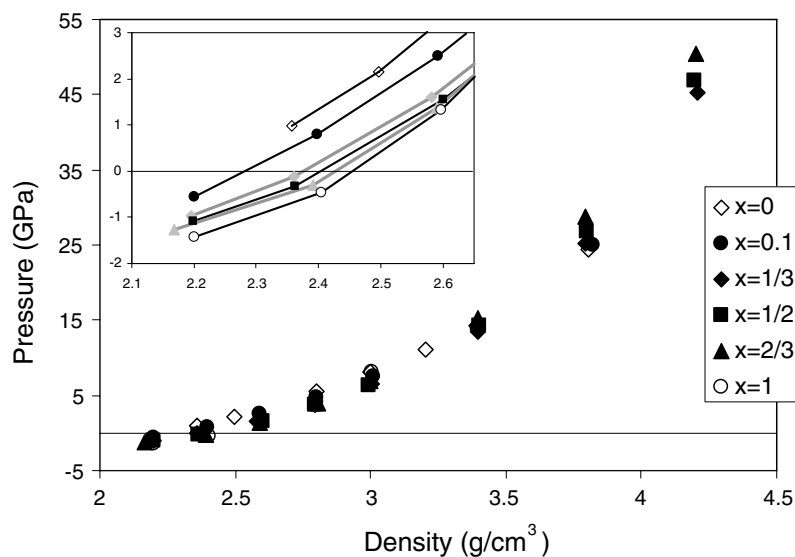


Fig. 4. Simulation results for the pressure as a function of density. Inset shows a close-up of results near zero pressure. The values of x represent the mole fraction of MgO in the system. Statistical errors are smaller than the size of the symbols.

Table 1
Property data derived from molecular dynamics simulations at 3000 K

Comp.	ρ (g/cm ³)	P (GPa)	D_{O} (10 ¹⁰ m ² /s)	D_{Si} (10 ¹⁰ m ² /s)	D_{Mg} (10 ¹⁰ m ² /s)	η (Pas)
SiO ₂	2.3565	0.98	0.16	0.089		4.9
	2.4974	2.14	0.37	0.21		0.69
	2.7991	5.49	1.99	1.32		0.38
	2.9972	8.13	4.39	2.96		0.17
	3.2037	11.1	7.78	5.53		0.038
	3.3925	14.3	9.58	6.82		0.024
	3.8029	24.3	6.83	5.30		0.027
	4.1998	41.2	2.21	1.76		0.17
MgSi ₉ O ₁₉	2.2003	−0.55	0.86	0.42	15.4	0.65
	2.3972	0.80	1.86	1.04	24.4	0.28
	2.5923	2.51	3.14	1.92	25.8	0.12
	2.7997	4.81	5.65	3.53	34.6	0.057
	3.0089	7.53	9.08	5.89	29.5	0.045
	3.3940	13.8	13.0	8.86	27.8	0.026
	3.8189	25.1	7.35	5.90	13.9	0.074
MgSi ₂ O ₅	2.1959	−0.98	7.70	4.56	72.7	0.045
	2.3602	−0.11	10.1	6.64	69.4	0.028
	2.5820	1.60	15.5	10.4	67.6	0.014
	2.7941	3.82	20.7	12.2	65.3	0.0071
	3.0018	6.50	22.0	15.8	61.5	0.011
	3.3978	13.6	20.4	14.0	41.9	0.019
	3.7946	25.3	10.1	6.68	20.3	0.024
	4.2063	45.3	2.06	1.39	4.34	0.39
MgSiO ₃	2.1980	−1.09	23.1	15.5	114	0.0098
	2.3624	−0.32	25.4	19.8	108	0.0068
	2.6012	1.54	30.9	20.7	105	0.0079
	2.7967	3.67	34.7	25.6	99.9	0.0069
	2.9943	6.39	35.4	24.4	79.9	0.0065
	3.4010	14.3	26.2	17.7	47.7	0.013
	3.7982	26.9	12.0	7.66	24.2	0.027
	4.1939	46.8	2.53	1.76	7.31	0.178
Mg ₂ SiO ₄	2.1678	−1.26	53.4	39.5	162	0.0033
	2.3907	−0.29	52.2	33.9	143	0.0035
	2.5907	1.37	51.5	35.8	130	0.0035
	2.8036	3.87	54.8	33.5	105	0.0044
	3.0016	6.87	47.4	31.9	97.6	0.0046
	3.3971	15.3	35.8	21.1	68.0	0.0078
	3.7932	28.8	12.5	10.7	16.9	0.024
	4.2042	50.4	3.71	2.75	13.0	0.10
MgO	2.2002	−1.43	172		217	0.0016
	2.4044	−0.46	142		222	0.0015
	2.5973	1.32	125		190	0.0025
	2.8013	4.14	99.6		151	0.0031
	3.0046	8.04	78.0		132	0.0034
	3.4071	19.3	50.4		91.8	0.0059

interpolation is used here. For pure SiO₂, extrapolation rather than interpolation is necessary, because the slow dynamics at low pressures precluded equilibration of states at negative pressure (for the viscosity and diffusivity, a linear extrapolation is carried out in terms of the log of the property). The state points used for these interpolations and extrapolations are shown in the inset of Fig. 4.

The results for the density at zero pressure and 3000 K are shown in Fig. 5a, and compared with available experimental results for SiO₂ (Lange and Carmichael, 1987) and MgSiO₃ (Courtial and Dingwell, 1999), extrapolated to 3000 K assuming a constant thermal expansion coefficient. The densities from the simulations are in excellent agreement with

the experimental results. However, such excellent agreement is clearly fortuitous; for example, the non-Coulombic sum is truncated here at 5.5 Å as described above, and if the non-Coulombic interaction were summed completely, a significantly greater density would be obtained.

Fig. 5b shows the molar volumes of the silicate melts, which can be considered as mixtures of SiO₂ and MgO. In the case of ideal mixing, the molar volume varies linearly with composition. The results in Fig. 5b show that the deviations from ideal mixing are significant, and are such that the excess volume of mixing is negative.

The results for the viscosity and diffusivity at zero pressure and 3000 K are shown in Fig. 6. The viscosity decreases

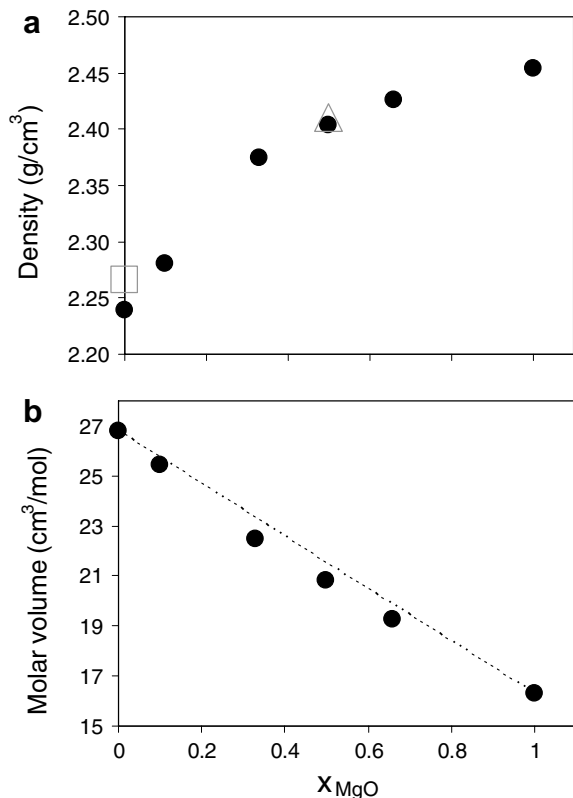


Fig. 5. Zero pressure results for the (a) density and (b) molar volumes as a function of composition. Statistical errors are smaller than the size of the symbols. Experimental results for the density at atmospheric pressure, extrapolated to 3000 K based on a linear thermal expansion coefficient, are shown as open symbols for SiO₂ (Lange and Carmichael, 1987) and MgSiO₃ (Courtial and Dingwell, 1999).

es, and the diffusivity increases, with increasing MgO content. These changes are very significant; the viscosity and the diffusivity of O and Si change by three orders of magnitude as x varies between 0 and 1. The diffusivity of Mg, a non-framework cation, is significantly greater than that of O and Si, especially in highly polymerized (SiO₂-rich) systems. The Mg diffusivity is also less dependent on the composition, and changes by only one order of magnitude as the composition changes. These results cannot be directly compared to experiment because experimental results are not available for these systems (with the exception of silica); however, the relationship of these results to experiments on other systems is addressed in the Discussion section.

3.2. High-pressure properties

The pressure dependence of the non-ideal mixing of SiO₂ and MgO is shown in Fig. 7. The excess molar volume, which is the difference between the actual molar volume and the molar volume based on ideal mixing, tends toward zero as the pressure increases. Note that data are restricted to pressures of 19 GPa or less, because beyond this pressure the pure MgO system partially crystallizes in the simulations.

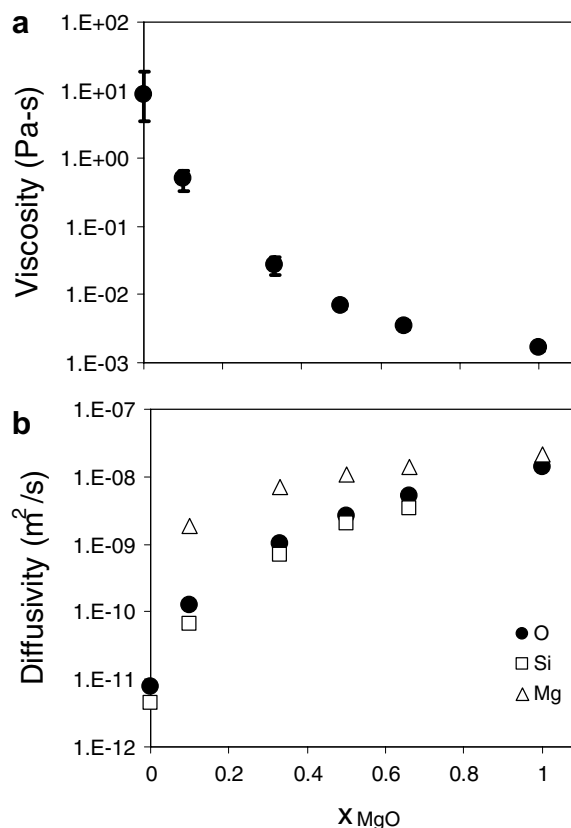


Fig. 6. Zero pressure results for (a) viscosity and (b) diffusivity as function of composition. When error bars are not visible, the statistical errors are smaller than the size of the symbols.

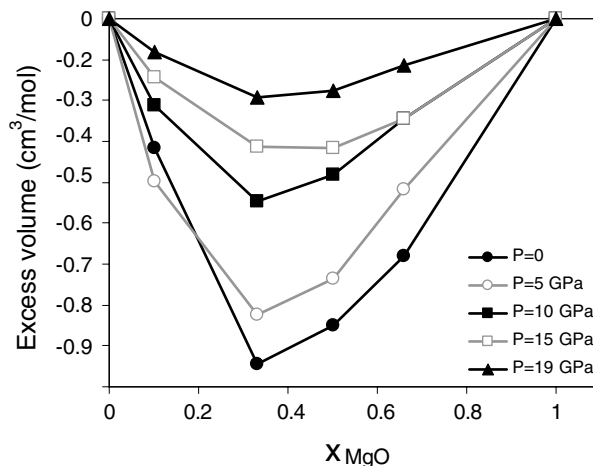


Fig. 7. Excess molar volumes as a function of composition, at various pressures. These results are obtained by interpolation of results at various fixed densities.

The pressure dependence of the viscosity and oxygen diffusivity are shown in Fig. 8. The MgO-rich systems behave ‘normally’, in that the viscosity increases with pressure and the diffusivity decreases with pressure. In contrast, the silica-rich (highly polymerized) systems behave ‘anomalously’, in that the viscosity initially decreases with pressure and the diffusivity initially increases with pressure. These composition-dependent pressure depen-

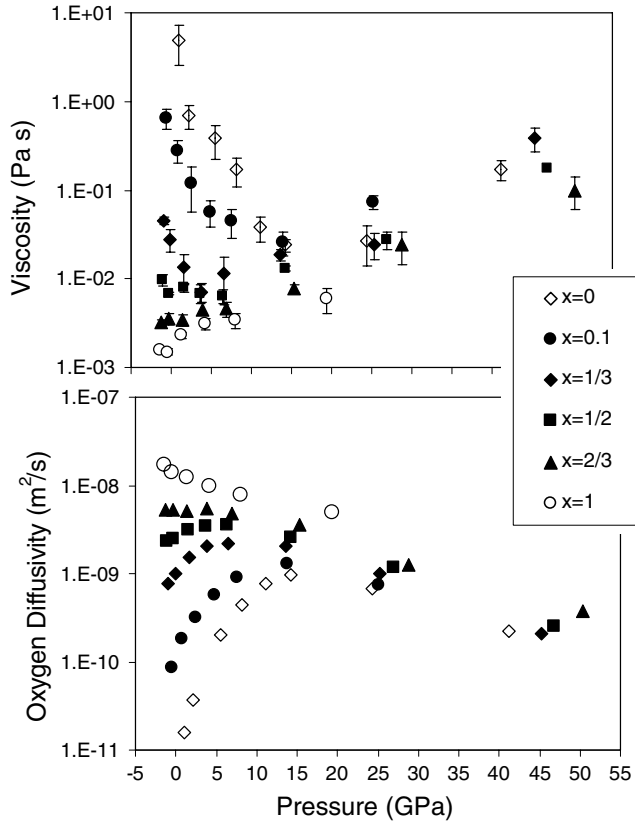


Fig. 8. Simulation results for viscosity and oxygen diffusivity as function of pressure. The values of x represent the mole fraction of MgO in the system. When error bars are not visible, the statistical errors are smaller than the size of the symbols.

dences concur with experimental observation (e.g., Scarfe et al., 1987; Behrens and Schulze, 2003).

At high pressures the viscosity and diffusivity become much more weakly dependent on composition. The viscosities and oxygen diffusivities as a function of composition at $P = 19$ GPa are compared with the zero-pressure results in Fig. 9. While these properties vary by over 3 orders of magnitude at zero pressure, they vary by less than 1 order of magnitude at 19 GPa.

Fig. 10 shows the diffusivities for Si and Mg in addition to O as functions of pressure and composition. The diffusivities for Si and O are similar, with Si diffusing slightly more slowly than O, and have similar dependences on pressure and composition. The diffusivity of Mg has a much smaller dependence on pressure: for the $x = 0.1$ system, the variations in the Mg diffusivity with pressure are an order of magnitude less than those for Si and O.

4. Discussion

4.1. Non-ideal mixing and partial molar volumes

The molar volume of a mixture can be expressed in terms of the partial molar volumes,

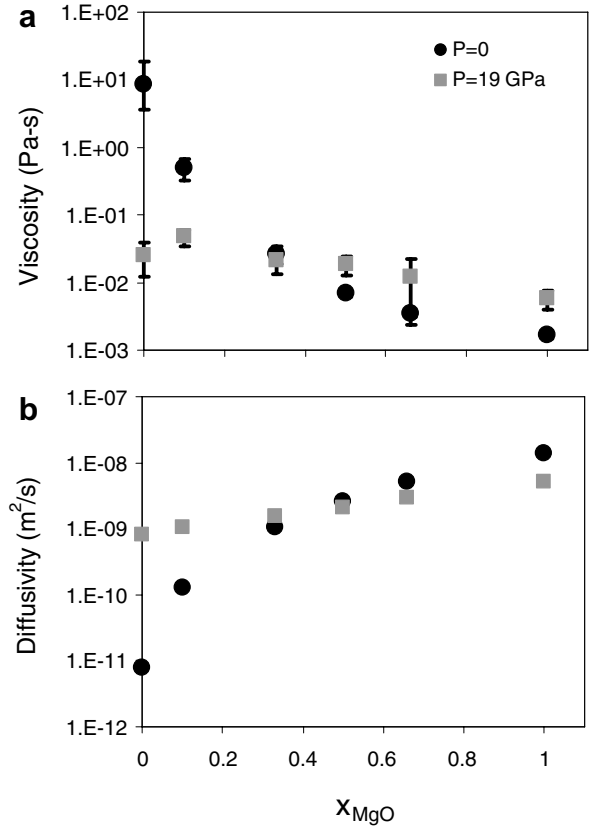


Fig. 9. Results at zero pressure and high pressure for (a) viscosity and (b) oxygen diffusivity as function of composition. When error bars are not visible, the statistical errors are smaller than the size of the symbols.

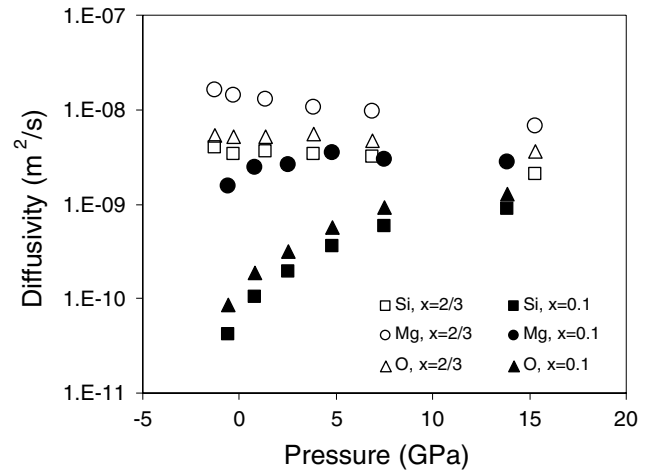


Fig. 10. Simulation results for diffusivities as a function of pressure, for a silica-rich and a silica-poor system. The values of x represent the mole fraction of MgO in the system. Statistical errors are smaller than the size of the symbols.

$$\bar{V} = \sum_i x_i \bar{V}_i(\{x\}) \quad (8)$$

where the partial molar volumes $\bar{V}_i = \left. \frac{\partial V}{\partial n_i} \right|_{n_{j \neq i}}$ are in general concentration dependent. A quadratic model is often used to approximate the molar volume,

$$\bar{V} = \sum_i x_i \bar{V}_i^0 + \sum_i \sum_{j>i} x_i x_j \bar{V}_{ij}^0 \quad (9)$$

where \bar{V}_i^0 is the molar volume of pure species i , and \bar{V}_{ij}^0 is an interaction term. Within this quadratic model, the partial molar volumes are given by

$$\bar{V}_i = \bar{V}_i^0 + \sum_j x_j^2 \bar{V}_{ij}^0. \quad (10)$$

Ideal mixing corresponds to the \bar{V}_{ij}^0 terms being equal to zero.

The non-ideality of mixing in the SiO₂–MgO system has not been effectively assessed experimentally because very high temperatures are necessary to study melts with high MgO content (Courtial and Dingwell, 1999). For this reason analyses have simply assumed that mixing in the MgO–SiO₂ system is ideal. However, experimental studies have shown that non-ideal mixing effects are significant in the CaO–SiO₂ system (Lange and Carmichael, 1987; Courtial and Dingwell, 1995, 1999). In particular, it was found that $\bar{V}_{\text{SiO}_2, \text{CaO}}^0 = -7.105 \text{ cm}^3/\text{mol}$ (Courtial and Dingwell, 1999), which is 34% of the value of \bar{V}_{CaO}^0 ($\bar{V}_{\text{CaO}}^0 = 20.664 \text{ cm}^3/\text{mol}$).

Molecular dynamics simulation can allow an assessment of the non-ideality of mixing in the SiO₂–MgO system. To carry out this assessment, the molar volume results (e.g., Fig. 5a) are fitted to the quadratic model (Eq. (10)); the resulting model parameters are given in Table 2. At zero pressure, it is found that $\bar{V}_{\text{SiO}_2, \text{MgO}}^0 = -3.24 \text{ cm}^3/\text{mol}$, which is 20% of the value of \bar{V}_{MgO}^0 ($\bar{V}_{\text{MgO}}^0 = 16.33 \text{ cm}^3/\text{mol}$).

Thus our MD simulations show that non-ideal effects are significant in terms of mixing in the MgO–SiO₂ system. While this conclusion is based on a crude force field for the Mg–O interaction, we note that the present result for the molar volume of liquid MgO at 3000 K, 16.3 cm³/mol, is very similar to a recent *ab initio* MD simulation result of 16.5 cm³/mol (Karki et al., 2006). For this reason we are confident in the reliability of this conclusion.

4.2. Viscosity and diffusivity in terms of structural modifier content

Giordano and Dingwell (2003) have shown that the viscosities of a wide range of silicate melts can be correlated based on the structural modifier (SM) content, which is the mole percentage of “structure modifying” oxides (i.e., all oxides other than SiO₂ and Al₂O₃). Our results are in quantitative agreement with their analysis of experimental

results. The viscosity has been measured experimentally for a wide range of silicate melts, but at temperatures less than 3000 K. To allow a comparison of the simulation results to experiment, the experimental results at lower temperature must be extrapolated to 3000 K. The temperature dependence of these properties is fit most effectively to a Vogel–Fulcher–Tammann (VFT) equation, which takes into account the non-Arrhenius variations with temperature (fragility) that usually characterize melt viscosities. VFT fits for a wide range of melts are given in the literature (Dingwell et al., 2004; Toplis and Dingwell, 2004; Russell and Giordano, 2005). For the diffusivity, VFT fits are unfortunately not available, and so only the Arrhenius equation can be used to extrapolate experimental diffusivities to 3000 K.

The simulation results for the viscosities and diffusivities are compared with experimental results for other systems in Fig. 11. The magnitudes of these properties, and their trends as a function of SM, are in good agreement with

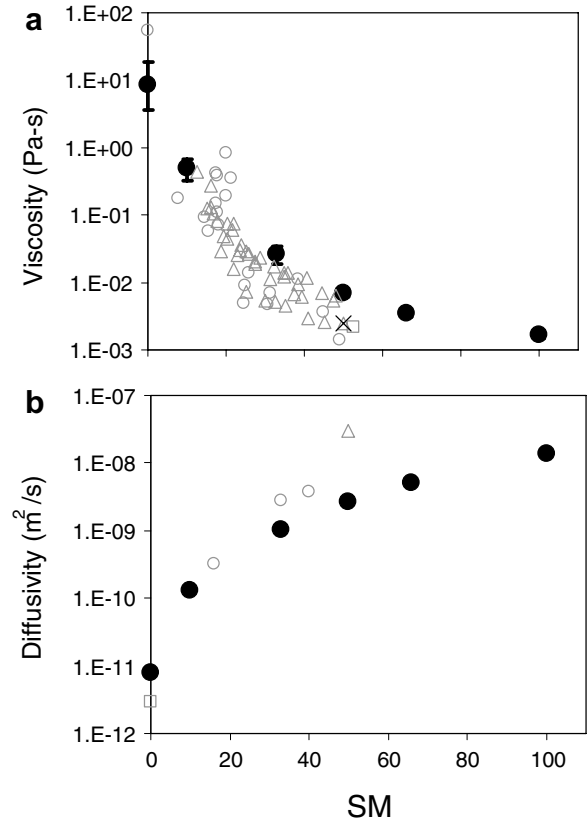


Fig. 11. Ambient pressure results for (a) viscosity and (b) oxygen diffusivity as function of structural modifier content. Filled symbols are our simulation results for the SiO₂–MgO join at 3000 K; when error bars are not visible, the statistical errors are smaller than the size of the symbols. Other symbols are experimental results for a range of compositions, extrapolated to 3000 K. The experimental results for the viscosity are extrapolated using the VFT equation with data as follows, circles, Giordano and Dingwell (2003); triangles, Russell and Giordano (2005); cross, Behrens and Schulze (2003); square, Dingwell et al. (2004). The experimental results for the diffusivity are extrapolated using the Arrhenius equation with data as follows, circles, Tinker et al. (2003); square, Mikkelsen (1984); triangle, Reid et al. (2001).

Table 2
Parameters that describe the mixing of SiO₂ and MgO (Eq. (9))

P (GPa)	$\bar{V}_{\text{SiO}_2}^0$ (cm ³ /mol)	\bar{V}_{MgO}^0 (cm ³ /mol)	$\bar{V}_{\text{SiO}_2, \text{MgO}}^0$ (cm ³ /mol)
0	26.73	16.33	−3.24
5	21.67	14.10	−2.53
10	19.14	13.04	−1.54
15	17.53	12.30	−1.26
19	16.73	11.79	−0.70

experimental results for a wide range of compositions. The mobility is somewhat overestimated (viscosity too low, diffusivity too high) at low SM and underestimated at high SM, which is likely a consequence of the approximate force field.

4.3. Relationship between viscosity and diffusivity

Equations that relate the viscosity and diffusivity have been widely used in the study of silicate melts (e.g., Shimizu and Kushiro, 1984; Poe et al., 1997; Reid et al., 2001; Mungall, 2002; Tinker et al., 2004). The utility of such equations is that a more easily measured quantity (which could be either viscosity or diffusivity, depending on the experimental conditions) could be used to determine the quantity that is more difficult to measure. The two most common of these equations are the Eyring and Stokes-Einstein relations, which are derived in completely different ways but relate the diffusivity and viscosity by the same functional form,

$$D\eta = \frac{kT}{\lambda} \quad (11)$$

The Eyring relation is derived from a phenomenological activated state description; λ is the jump distance for a diffusive event, which is often considered to be equal to the diameter of one of the diffusing species, $\lambda = 2R$. The Stokes-Einstein relation is derived from consideration of the Brownian motion of a macroscopic sphere moving slowly through a fluid; $\lambda = 4\pi R$ for a free-slip fluid-sphere boundary, and $\lambda = 6\pi R$ for the case of a no-slip boundary.

These relations have been examined in silicate melts, based on the oxygen diffusivity. Some investigations have found that $\lambda = 2R_O$, where the radius of oxygen was taken as 1.4 Å, gives a good correlation between the viscosity and the oxygen diffusivity (Shimizu and Kushiro, 1984; Poe et al., 1997). However, other investigations found that larger values of λ are necessary to correlate the viscosity and diffusivity, e.g., $\lambda \approx 4R_O$ (Tinker et al., 2004). These investigations were for melts of different compositions, and so it was not clear whether the different values of λ accounted for different mechanisms of diffusion and viscous stress relaxation – e.g., larger values of λ were found for depolymerized melts.

The relevance of the Eyring/Stokes-Einstein equations is addressed with the present simulation results. Fig. 12 shows the value of $\lambda = kT/D\eta$ for the silicate melts at zero pressure. The simulation results yield values of λ between $4R_O$ and $16R_O$ (using $R_O = 1.4$ angst), where the value of λ increases with increasing MgO content. This result agrees with the experimental observation that the values of λ are larger for depolymerized melts (Tinker et al., 2004).

Experiments on room temperature liquids, which are more precise than those on silicate melts (because the experiments can be carried out at room temperature), support the relevance of these values of λ . In particular, experiments on tetramethyl silane and benzene find λ in the

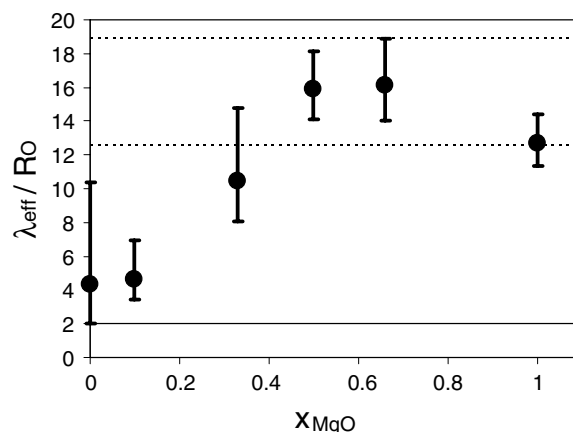


Fig. 12. Values of λ that relate the viscosity and diffusivity (Eq. (11)). The solid line is the Eyring model value with jump length equal to the ionic diameter of oxygen, and the dashed lines are the Stokes-Einstein values with slip (lower line) and no-slip (upper line).

range $12R$ to $16R$, i.e., the range predicted by the Stokes-Einstein relation (Parkhurst and Jonas, 1975). Furthermore, molecular simulations of a Lennard-Jones system also find λ to be in the range $12R$ to $16R$ (Lacks, 2002). These liquids can be considered depolymerized, and the values of λ are in the same range as the values obtained for depolymerized liquids in our simulations. Tentatively, it appears that values of λ below the range predicted by the Stokes-Einstein relation are obtained only in relatively highly polymerized silicate liquids. Whether this observation has any significance in terms of liquid structure is unclear, since these relations are phenomenological rather than rigorous.

4.4. Properties at high pressure

The effects of pressure were investigated in regard to the volumes of mixing, viscosities and diffusivities. At higher pressure, it is found that: (1) The excess volume of mixing decreases (see Fig. 7), so that the mixing is more ideal; and (2) The viscosity and diffusivity at high pressure becomes much more weakly dependent on composition (see Fig. 9). These two effects are likely related. The viscosity and diffusivity results show that the SiO₂ and MgO systems become more similar at higher pressures. Because the systems are more similar, it is expected that they would mix more ideally.

The likely origin of these two effects is that the structures of the SiO₂ and MgO systems become more similar at high pressure. At low pressure, the structures are very different, in that the SiO₂ has an open framework structure while MgO has a close-packed structure. However, with increasing pressure, the SiO₂ structure becomes closely packed as well.

5. Conclusions

Molecular dynamics simulations were performed on six compositions along the MgO–SiO₂ join at 3000 K and

pressures up to 50 GPa. The densities obtained from the simulations are consistent with available experimental data, and viscosities and chemical diffusivities are in quantitative agreement with experimental results for silicate melts with the same content of structure modifying oxides. The viscosities of low-SiO₂ liquids increase with pressure, while the viscosities of high-SiO₂ liquids decrease initially, then increase at higher pressures. Si and O diffusion coefficients show similar behavior, and the results are consistent with the Eyring equation relating diffusivity and viscosity. Viscosities and oxygen diffusivities vary over three orders of magnitude between pure MgO and pure SiO₂ systems at zero pressure, but by only a factor of ~3 at pressures of ~15 GPa or higher. MgO and SiO₂ exhibit non-ideal mixing behavior with a negative excess volume of mixing at zero pressure, but at higher pressures the excess volume approaches zero. Our results indicate that liquids in the MgO–SiO₂ system become more similar to each other at high pressure, leading their transport properties to converge to similar values and their mixing behavior to become more ideal. If this holds true generally for natural multi-component silicate melts, extrapolation of their property data to pressures of Earth's deep mantle may be greatly simplified.

Acknowledgments

We thank Michael-Paul Robinson for calculating the radial distribution functions that demonstrated the crystallization of MgO at high pressures, and an anonymous reviewer for suggestions that improved the manuscript.

Associate editor: Claudia Romano

References

- Abe, Y., 1997. Thermal and chemical evolution of the terrestrial magma ocean. *Phys. Earth Planet. Inter.* **100**, 27–39.
- Allen, M.P., Tildesley, D.J., 1989. *Computer Simulation of Liquids*. Clarendon, Oxford, UK.
- Behrens, H., Schulze, F., 2003. Pressure dependence of melt viscosity in the system NaAlSi₃O₈–CaMgSi₂O₆. *Am. Mineral.* **88**, 1351–1363.
- Courtial, P., Dingwell, D.B., 1995. Nonlinear composition dependence of molar volume of melts in the CaO–Al₂O₃–SiO₂ system. *Geochim. Cosmochim. Acta* **59**, 3685–3695.
- Courtial, P., Dingwell, D.B., 1999. Densities of melts in the CaO–MgO–Al₂O₃–SiO₂ system. *Am. Mineral.* **84**, 465–476.
- Dingwell, D.B., Courtial, P., Giordano, D., Nichols, A.R.L., 2004. Viscosity of peridotite liquid. *Earth Planet. Sci. Lett.* **225**, 127–138.
- Giordano, D., Dingwell, D.B., 2003. Non-Arrhenian multicomponent melt viscosity: a model. *Earth Planet. Sci. Lett.* **208**, 337–349.
- Horbach, J., Kob, W., 1999. Static and dynamic properties of a viscous silica melt. *Phys. Rev. B* **60**, 3169–3181.
- Karato, S.-I., Murthy, V.R., 1997. Core formation and chemical equilibrium in the Earth, I. Physical considerations. *Phys. Earth Planet. Inter.* **100**, 61–79.
- Karki, B.B., Bhattarai, D., Stixrude, L., 2003. First-principles calculations of the structural, dynamical, and electronic properties of liquid MgO. *Phys. Rev. B* **73**, Art. No. 174208.
- Lacks, D.J., 1998. Localized mechanical instabilities and structural transformations in silica glass under high pressure. *Phys. Rev. Lett.* **80**, 5385–5388.
- Lacks, D.J., 2002. Stokes-Einstein-like relation for athermal systems and glasses under shear. *Phys. Rev. E* **66**, 051202.
- Lange, R.A., Carmichael, I.S.E., 1987. Densities of Na₂O–K₂O–CaO–MgO–FeO–Fe₂O₃–Al₂O₃–TiO₂–SiO₂ liquids: new measurements and derived partial molar properties. *Geochim. Cosmochim. Acta* **51**, 2931–2946.
- Lay, T., Garner, E.J., Williams, Q., 2004. Partial melting in a thermochemical boundary layer at the base of the mantle. *Phys. Earth Planet. Inter.* **146**, 441–467.
- Leshner, C.E., Hervig, R.L., Tinker, D., 1996. Self diffusion of network formers (silicon and oxygen) in naturally occurring basaltic liquid. *Geochim. Cosmochim. Acta* **60**, 405–413.
- Liebske, C., Schmickler, B., Terasaki, H., Poe, B.T., Suzuki, A., Funakoshi, K.-I., Ando, R., Rubie, D.C., 2005. Viscosity of peridotite liquid up to 13 GPa: implications for magma ocean viscosities. *Earth Planet. Sci. Lett.* **240**, 589–604.
- McDonough, W.F., Sun, S.S., 1995. The composition of the Earth. *Chem. Geol.* **120**, 223–253.
- Mikkelsen Jr., J.C., 1984. Self diffusivity of network oxygen in vitreous SiO₂. *Appl. Phys. Lett.* **45**, 1187–1189.
- Mungall, J.E., 2002. Empirical models relating viscosity and tracer diffusion in magmatic silicate melts. *Geochim. Cosmochim. Acta* **66**, 125–143.
- Mysen, B.O., 1988. *Structure and Properties of Silicate Melts*. Elsevier, Amsterdam, 354 pp.
- Parkhurst Jr., H.J., Jonas, J., 1975. Dense liquids. II. The effect of density and temperature on viscosity of tetramethylsilane and benzene. *J. Chem. Phys.* **63**, 2705–2709.
- Poe, B.T., McMillan, P.F., Rubie, D.C., Chakraborty, S., Yarger, J., Diefenbacher, J., 1997. Silicon and oxygen self diffusivities in silicate liquids measured to 15 gigapascals and 2800 kelvin. *Science* **276**, 1245–1248.
- Reid, J.E., Poe, B.T., Rubie, D.C., Zotov, N., Wiedenbeck, M., 2001. The self-diffusion of silicon and oxygen in diopside (CaMgSi₂O₆) liquid up to 15 GPa. *Chem. Geol.* **174**, 77–86.
- Reid, J.E., Suzuki, A., Funakoshi, K.-I., Terasaki, H., Poe, B.T., Rubie, D.C., Ohtani, E., 2003. The viscosity of CaMgSi₂O₆ liquid at pressures up to 13 GPa. *Phys. Earth Planet. Inter.* **139**, 45–54.
- Rubie, D.C., Melosh, H.J., Reid, J.E., Liebske, C., Richter, K., 2003. Mechanisms of metal-silicate equilibration in the terrestrial magma ocean. *Earth Planet. Sci. Lett.* **205**, 239–255.
- Russell, J.K., Giordano, D., 2005. A model for silicate melt viscosity in the system CaMgSi₂O₆–CaAl₂Si₂O₈–NaAlSi₃O₈. *Geochim. Cosmochim. Acta* **69**, 5333–5349.
- Saika-Voivod, I., Sciortino, F., Poole, P.H., 2001. Computer simulations of liquid silica: equation of state and liquid-liquid phase transition. *Phys. Rev. E* **63**, Art. No. 011202.
- Scarfe, C.M., Mysen, B.O., Virgo, D., 1987. Pressure dependence of the viscosity of silicate melts. In: Mysen, B.O. (Ed.), *Magmatic processes: physicochemical principles*, The Geochemical Society Spec. Publ. 1. University Park, Pennsylvania, pp. 59–67.
- Shimizu, N., Kushiro, I., 1984. Diffusivity of oxygen in jadeite and diopside melts at high pressures. *Geochim. Cosmochim. Acta* **48**, 1295–1303.
- Speziale, S., Zha, C.-S., Duffy, T.S., Hemley, R.J., Mao, H.-K., 2001. Quasi-hydrostatic compression of magnesium oxide to 52 GPa: implications for the pressure–volume–temperature equation of state. *J. Geophys. Res.* **106**, 515–528.
- Stixrude, L., Karki, B., 2005. Structure and freezing of MgSiO₃ liquid in Earth's lower mantle. *Science* **310**, 297–299.
- Suzuki, A., Ohtani, E., Funakoshi, K., Terasaki, H., Kubo, T., 2002. Viscosity of albite melt at high pressure and high temperature. *Phys. Chem. Miner.* **29**, 159–165.
- Tinker, D., Leshner, C.E., 2001. Self diffusion of Si and O in dacitic liquid at high pressures. *Am. Mineral.* **86**, 1–13.

- Tinker, D., Leshner, C.E., Hutcheon, I.D., 2003. Self-diffusion of Si and O in diopside-anorthite melt at high pressures. *Geochim. Cosmochim. Acta* **67**, 133–142.
- Tinker, D., Leshner, C.E., Baxter, G.M., Uchida, T., Wang, Y., 2004. High-pressure viscometry of polymerized silicate melts and limitations of the Eyring equation. *Am. Mineral.* **89**, 1701–1708.
- Toplis, M.J., Dingwell, D.B., 2004. Shear viscosities of CaO–Al₂O₃–SiO₂ and MgO–Al₂O₃–SiO₂ liquids: implications for the structural role of aluminum and the degree of polymerization of synthetic and natural aluminosilicate melts. *Geochim. Cosmochim. Acta* **68**, 5169–5188.
- van Beest, B.W.H., Kramer, G.J., van Santen, R.A., 1990. Force fields for silicas and aluminophosphates based on ab initio calculations. *Phys. Rev. Lett.* **64**, 1955–1958.
- Van Orman, J.A., Fei, Y., Hauri, E.H., Wang, J., 2003. Diffusion in MgO at high pressures: constraints on deformation mechanisms and chemical transport at the core-mantle boundary. *Geophys. Res. Lett.* **30**, 1056.